IONS® Karlsruhe 2015

International OSA Network of Students

26 – 29 June 2015

Abstract Collection

Oral Presentations

INTERNATIONAL
YEAR OF LIGHT
2015

SKar
Optics Students Karlsruhe

IONS®
International OSA
Network of Students

OSA®
The Optical Society

International OSA Network of Students

IONS® Karlsruhe 2015

26 – 29 June 2015

Karlsruhe Institute of Technology, Karlsruhe, Germany

Editors:

Daria D. Bezshlyakh

Radwanul Hasan Siddique

Optics Students Karlsruhe e.V., International Department of Karlsruhe Institute of Technology,

76131 Schlossplatz 19, Karlsruhe, Germany

http://ionskarlsruhe.osahost.org/

pr@optics-karlsruhe.de

Conference organized in with support of The Optical Society and Karlsruhe School of Optics and Photonics

Mehmet Can Kerse, Bilkent University, Turkey
"Non-thermal High Speed Tissue Processing Using a Burst Mode Ultra-Short Pulsed Fiber Laser System"

Ulas Sabahattin Gokay, Koc University, Turkey
"Fano Resonances of a Silicon Microsphere on a Silica Optical Fiber Coupler"

Nickolay Schedrin, Bauman Moscow State Technical University, Russia
"Supercontinuum Generation in Microstructured Fiber with Different Anomalous Dispersion near Zero-Dispersion Wavelength"

Ruben Huenig, Karlsruhe Institute of Technology, Germany
"Multifunctional Dual-Scale Biomimetic Structures for Solar Cell Application"

Sonika Obheroi, Vellore Institute of Technology, India
"Design and Analysis of Holographic Solar Concentrator for Semiconductor Electrodes for Photoelectrochemical Hydrogen Production Device"

Achim Woessner, The Institute of Photonic Sciences, Spain
"Near-field Photocurrent as Characterization Tool for Graphene Devices"

Anna Ovvyan, Karlsruhe Institute of Technology, Germany
"Tunable Mach-Zehnder Interferometers Made of Silicon Nitride-on-Insulator Substrates"

Christian Kneis, University of Bordeaux, France
"Mid-Infrared Supercontinuum Generation in a Fluoride Fiber from an Actively Q-switched Mode-Locked Tm3+-doped Silica Fiber Laser"

Mohammadreza Oraie, Shahid Beheshti University, Iran
"Electromagnetic Simulation of On-chip Optofluidic Devices: liquid core/liquid cladding waveguides"

Zhanna Rodnova, Bauman Moscow State Technical University, Russia
"Study of Scintillating Fibers Optical Properties"

Mehdi Alem, École Polytechnique Fédérale de Lausanne, Switzerland
"Random Telegraph Signal vsRandom BinarySequence for Suppressing the Stimulated Brillouin Backscattering"

Ali Shahpari, University of Aveiro, Portugal
"Next Generation Optical Access Networks: Technologies and Economics"

Mateusz Szatkowski, Wroclaw University of Technology, Poland
"Optical Vortex Response due to Specified Phase Disturbance"

Atharva Sahasrabudhe, Indian Institute of Science Education and Research, India
"Core/Shell/Quasi-Shell Quantum Dot Absorbers: A Dual Sensitization Strategy for High Performance Photovoltaics"

Diaa Ahmed Mohamed Ahmedien, University of Bern, Graduated school of Arts, Bern, Switzerland
"Use Mechanisms of the Holographic Interferometry in Sciences of Visual Arts: Analytical Theoretical Study"
Ahmet Turnali, Bilkent University, Turkey
"Direct Laser Writing of Volume Fresnel Zone Plates in Silicon"

Abel Gil Villalba, Intitut FEMTO-ST, France
"Single Pulse Ultrafast Laser Sub-Micron Ablation of Graphene"

Sambit Mitra, Karlsruhe Institute of Technology, Germany
"Micro-Channel Machining Using High-Energy Femtosecond Bessel Beams"

Marta Lange, University of Latvia, Latvia
"Determining the Bilirubin Concentration in Bruises of Human Skin Using Spectral Imaging"

Sviatoslav Gusev, ITMO University, Russia
"Investigation of Glucose Level Influence on Blood Optical Properties in THz Frequency Range"

Eliel Silva Neto, Universidade Federal de Minas Gerais, Brasil
"Raman Spectroscopy in Twisted Bilayer Graphene"

Non-thermal High Speed Tissue Processing Using a Burst Mode Ultra-Short Pulsed Fiber Laser System

Can Kerse[1,*], Seydi Yavaş[2, 3], Hamit Kalaycıoğlu[4], Mehmet D. Aşık[5], Önder Akçaalan[4], F. Ömer Ilday[1, 2, 4]

[1]Department of Electrical and Electronics Engineering, Bilkent University, Ankara, 06800, Turkey
[2]UNAM - Institute of Materials Science and Nanotechnology, Bilkent University, Ankara, 06800, Turkey
[3]FiberLAST, Inc., Ankara, 06531, Turkey
[4]Department of Physics, Bilkent University, Ankara, 06800, Turkey
[5]Nanotechnology and Nanomedicine Department, Institute of Science, Hacettepe University, Ankara, 06800, Turkey

Corresponding author: cankerse@ee.bilkent.edu.tr

Femtosecond pulses hold great promise for high-precision tissue removal. However, ablation rates are severely limited by the need to keep average laser power low to avoid collateral damage due to heat accumulation [1]. Furthermore, previously reported pulse energies preclude delivery in flexible fibers, hindering in vivo operation. Both of these problems can be addressed through use of groups of high-repetition-rate pulses, or bursts [2 - 3]. Here, we report a novel fiber laser and demonstrate ultrafast burst-mode ablation of brain tissue at rates approaching 1 mm^3/min, an order of magnitude improvement over previous reports. Burst mode operation is shown to be superior in terms of energy required and avoidance of thermal effects, compared to uniform repetition rates. These results can pave the way to in vivo operation at medically relevant speeds, delivered via flexible fibers to surgically hard-to-reach targets, or with simultaneous magnetic resonance imaging. Here, we show a custom built laser specifically built in order to overcome these limitations and represent histology results with no collateral damage.

The system produces up to 8 µJ pulses with ~300 fs FWHM pulse duration at 200 kHz uniform pulse rep. rate or 22.3 MHz intra-burst pulse rep. rate with 50 KHz inter-burst repetition rate. Freshly harvested rat brain tissues, which were processed within an hour after dissection were used during the experiments, where we tested the effect of these two operating modes. The pulse energy on sample was kept at 3 µJ. We performed raster scans over an area of 1 mm x 1 mm. After irradiation, the samples were preserved in 4% paraformaldehyde solution, and then examined with a micro-CT scanner (Skyscan 1172, Bruker). For histological analyses, following fixation, the tissue samples were embedded into paraffin blocks and then cut into 5 µm slices in sagittal plane, perpendicular to tissue surface. Then, slices were examined under light microscopy (Leica, DM 5000 B) following a standard hemotoxylin-eosin staining procedure. The experimental setup is depicted in Fig.1 including the laser stage and the material processing stage. Fig. 1 shows the temporal profile of two operating modes together with micro-CT and histology results.

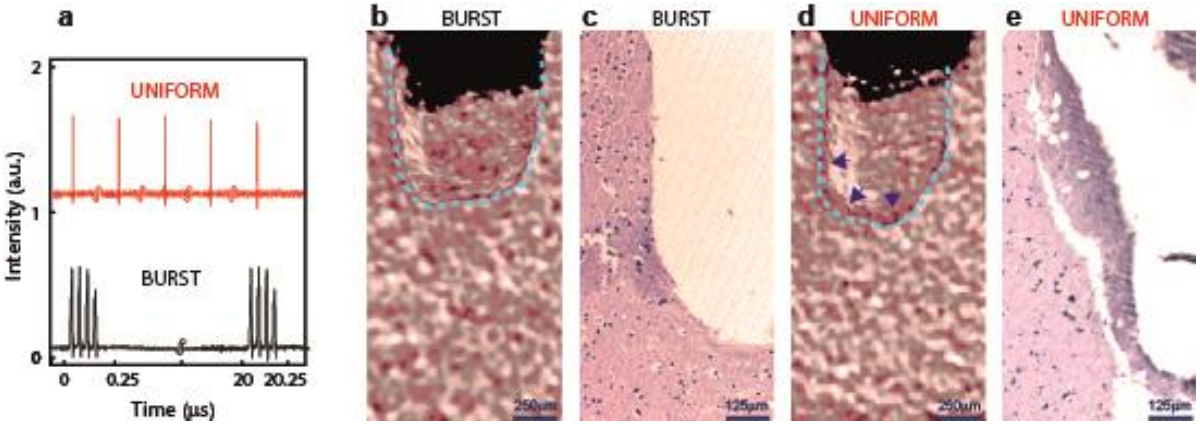

Fig. 1 The temporal profile, micro-CT sections and histological appearances of burst and uniform mode operations. (a) Temporal profile of burst and uniform modes. (b) Micro-CT section of rat brain tissue sample ablated with burst mode. (c) Histological section of b. (d) Micro-CT section of rat brain tissue sample ablated with uniform mode. (e) Histological section of d.

Histological analysis reveals that large areas have been heat-affected for uniform-mode ablation, as compared to burst-mode operation. The results obtained by the application of ~50 times lower pulse energies than it is in literature with solid state lasers. This is promising for delivery in flexible and low-loss photonic crystal fibers to remote parts of the body.

References

[1] A. Vogel, J. Noack, G. Huttman and G. Paltauf, "Mechanisms of femtosecond laser nanosurgery of cells and tissues," Appl. Phys. B¨ **81**, 1015 - 1047 (2005)

[2] R.S. Marjoribanks, et.al. "Ablation and thermal effects in treatment of hard and soft materials and biotissues using ultrafast-laser pulse-train bursts", Photon.Lasers Med. **1**, 155-169 (2012)

[3] C. Kerse, H. Kalaycıoglu, F.˙ O. Ilday, E. Atalar, "Non-thermal Material and Tissue Processing with 100 MHz and 500 MHz Repetition Rate Bursts", CLEO Europe-OSA Technical Digest (2013)

Fano Resonances of a Silicon Microsphere on a Silica Optical Fiber Coupler

Ulaş Sabahattin Gökay[1], Muhammad Zakwan[1], Abdullah Demir[2] and Ali Serpengüzel[1]

[1]*Koç University, Microphotonics Research Laboratory, Department of Physics, Rumelifeneri Yolu, Sarıyer, Istanbul 34450 Turkey*

[2]*JDSU Corporation, 80 Rose Orchard Way, San Jose, California 95134 USA*

ugokay@ku.edu.tr

In previous decades, Lorentzian and Fano lineshapes in optical resonances have been observed in optical microcavities [1, 2]. In this work, we present asymmetrical Fano lineshape whispering gallery modes (WGMs) in 90° elastic scattering from a silicon microsphere. Our experimental setup is shown in Fig.1 (a), where the inset shows the phase relation between the input and the WGMs observed in the 90° scattering and 0° transmission. An optical fiber half coupler (OFHC) is used to excite the WGMs of the silicon microsphere, where a distributed feedback (DFB) laser is used as a tunable light source. The analysis of the experimental spectra in Fig.1 (b) shows that the polar angular mode spacing of 0.23 nm correlates well with the calculated mode spacing of the WGMs. The measured effective quality factor (Q) of the Fano resonance is on the order of 10^5, which can be further improved with appropriate choice of experimental setup parameters. In order to analyze the experimental results, we used the transfer matrix method, which couples the optical fiber mode and two separate WGMs in the microsphere. The coupling of two WGMs in a single microsphere is thus related by the transfer matrix between field amplitudes using the coupling parameters. The complex electrical field amplitudes are used as the input and output entries, whereas the coupling and transmission coefficients constitute the 3×3 transfer matrix. In our analysis with the transfer matrix, the cross coupling of the 1st and the 2nd WGMs leads to Lorentzian or Fano lineshapes depending on the relative phase difference between the WGMs. With the use of improved interface designs and optimized coupling methods to silicon microspheres, Fano resonances herald novel microcavity based optoelectronic switches [3], add-drop filters [4], and modulators [5] for future photonic lightwave circuits.

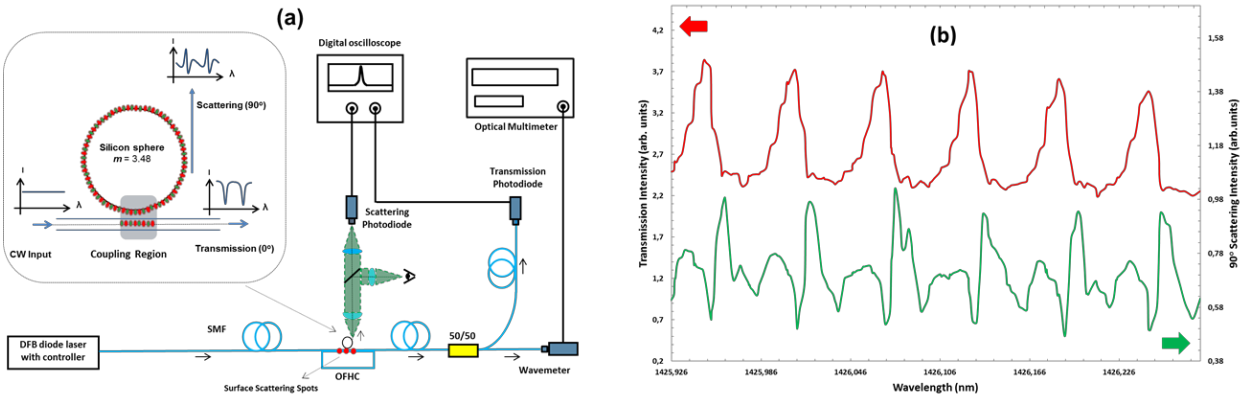

Fig. 1 (a) The schematic of the experimental setup and (b) WGMs observed in 0° transmission and 90° scattering of the silicon microsphere.

References

[1] Y. Lu, J. Yao, X. Li, and P. Wang, "Tunable asymmetrical Fano resonance and bistability in a microcavity-resonator-coupled Mach-Zehnder interferometer," Opt. Lett. **30**, 3069 (2005).

[2] L. Zhou and A. W. Poon, "Fano resonance-based electrically reconfigurable add–drop filters in silicon microring resonator-coupled Mach–Zehnder interferometers," Opt. Lett. **32**, 781 (2007).

[3] D. O'Shea, C. Junge, M. Pöllinger, A. Vogler, and A. Rauschenbeutel, "All-optical switching and strong coupling using tunable whispering-gallery-mode microresonators," Appl. Phys. B **105**, 129-148 (2011).

[4] W. Ding, B. Luk'yanchuk, and C.-W. Qiu, "Ultrahigh-contrast-ratio silicon Fano diode," Phys. Rev. A **85**, 025806 (2012).

[5] L. Y. Mario, S. Darmawan and M. K. Chin, "Asymmetric Fano resonance and bistability for high extinction ratio, large modulation depth, and low power switching," Opt. Exp. **14**, 12770-12781 (2006).

Supercontinuum Generation in Microstructured Fiber with Different Anomalous Dispersion near Zero-Dispersion Wavelength

Nickolay Schedrin[1*], Stanislav Leonov[1], Vladimir Lazarev[1], and Valeriy Karasik[1]

[1] *Scientific-Educational Center "Photonics and IR-Technology" of Bauman Moscow State Technical University, 5/1, 2nd Baumanskaya str., Moscow, 105005, Russia*

***Corresponding author:** nickolaj95@gmail.com*

Supercontinuum (SC) generation in microstructured fibers or also called photonic crystal fibers (PCFs) has been under close attention since it was firstly demonstrated [1, 2]. SC generation in PCFs by using only low intensity Ti:Sapphire femtosecond pulses with normal and anomalous-dispersion has been a goal of many researcher efforts [3, 4]. High spatial brightness and coherently pulsed nature of SC generated in PCFs makes it an ideal source for a lot of applications, for example, fs-pulse phase stabilization, frequency metrology [5], optical coherence tomography, spectroscopy of materials and etc. Also parameters of SC generated in PCF can be changed by filling the PCF holes with nonlinear media [6]. The goal of this paper is to present the results of experimental studies of SC generation in microstructured fiber under different anomalous-dispersion regime near zero-dispersion wavelength (ZDW).

A microstructured fiber was produced by Fiber Optics Research Center of RAS. A dispersion curve and cross-section of the fiber is presented in Fig. 1(a). The main parameters of the fiber are: core diameter is equal to 2 μm, hole diameter (d) is 3 μm and pitch (Λ) is 3.2 μm. We measured the SC generation spectra as a function of pump wavelength (λ_p) and pump power. Figure 1b shows two experimental spectra for different pump wavelengths at pump power 72 mW.

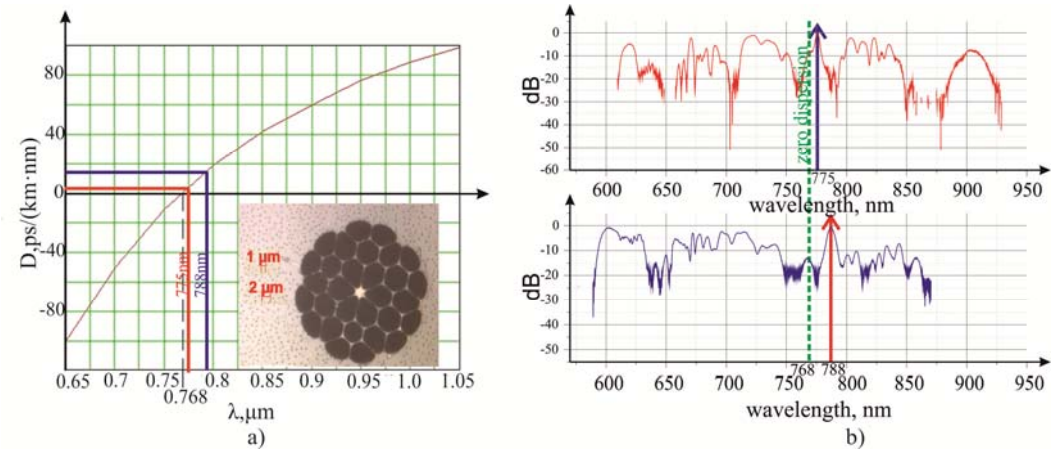

Fig. 1 (a) Dispersion curves. Inset: the fiber cross-section. (b) Recorded spectra for two pump wavelengths: λ_p = 775 nm, 788 nm.

It can be seen from Figure 1(b) that widest spectrum was observed, when pump wavelength was 775 nm. The output radiation was bright with rich orange colour. Measurements of the SC spectra as a function of pump power show that with pump power larger than 50mW the output spectrum width started being lower. We assume that this dependence can be caused by not an ideal longitudinal structure of PCF.

References

[1] W. J. Wadsworth, A. Ortigosa-Blanch, J. C. Knight, T. A. Birks, T. P. M. Man, and P. St. J. Russell, "Supercontinuum generation in photonic crystal fibers and optical fiber tapers: a novel light source," *JOSA B* **19**, 2148–2155 (2002).

[2] Dudley J.M., Genty G., Coen S, "Supercontinuum generation in photonic crystal fiber," *Rev. Mod. Phys.* **78**, 1135–1184 (2006).

[3] J. K. Ranka, R. S. Windeler, and A. J. Stentz, ''Visible continuum generation in air-silica microstructure fibers with anomalous dispersion at 800 nm,'' *Opt. Lett.* **25**, 25–27 (2000).

[4] Zhang S, Yang X, Lu F, Gong Y, Meng X "Supercontinuum generation in photonic crystal fibers with a normal dispersion pump pulse near the zero-dispersion wavelength," *Opt. Eng.* **47**, 075005 (2008).

[5] A. Benedick, D. Tyurikov, M. Gubin, R. Shewmon, I. Chuang, and F. Kartner, "Compact, Ti:sapphire-based, methane-stabilized optical molecular frequency comb and clock," *Opt. Lett.* **34**, 2168-2170 (2009).

[6] I. N Dolganova, K. I Zaytsev, S. O Leonov, A. O Schadko, K. A Komarov and S. O Yurchenko "Nonlinear conversion in optical waveguide filled with NaNO2," *J. Phys.: Conf. Ser.* **584**, 012009 (2015).

Multifunctional dual-scale biomimetic structures for solar cell application

R. Hünig,[1] M. Stephan,[1] G. Gomard,[1] O. Kiowski,[2] U. Lemmer,[1] and M. Powalla[1,2]

[1]*Light Technology Institute (LTI), Karlsruhe Institute of Technology (KIT), Engesserstraße 13, 76131 Karlsruhe*
[2]*Center for Solar Energy and Hydrogen Research (ZSW), Industriestr. 6, 70565 Stuttgart*
***Corresponding author:** Ruben.Huenig@kit.edu*

In the field of optics and photonics bionics have seen a growing interest, e.g. as sub-wavelength structures imitating the moth-eye's hull leading to highly anti-reflective surfaces [1-3]. So far, attention has been mainly focused on animal kingdom and on nano-scale structures. However, recent studies based on lithography and dry etching processes have shown that combining nano and micro-structures could further decrease the reflection [4,5]. As highlighted by Schulte et al. some plants display such dual-scale surfaces that exhibit low reflection, strong forward scattering and super-hydrophobicity, thus making them potential prototypes for solar module surfaces [6].

We report here on the properties of plants' dual scale surface structures regarding their aptitude for solar cells. The precise replication onto CIGS solar cells is done by a soft imprint lithography technique. Subsequent integrated reflection measurements show a significant reduction of the reflected light under all angles of incidence (AOI) compared to a flat surface, evidencing only 1 % reflection for AOI close to the normal and 8 % for an AOI of 80° for a rose-inspired surface (Fig.1). According to these measurements, average reflection losses are reduced by almost 75 %.

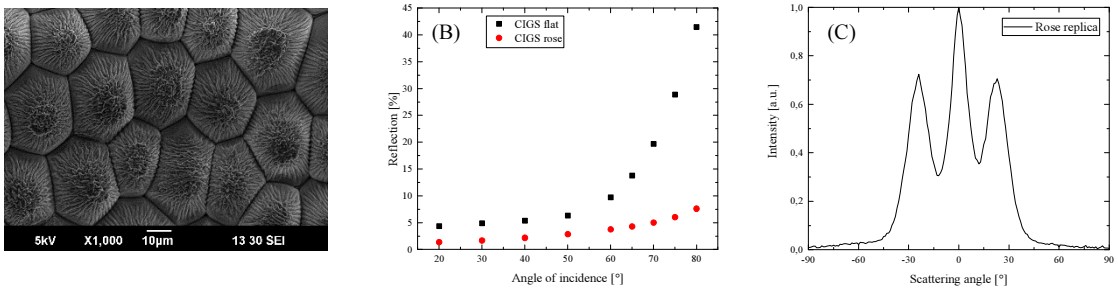

Fig. 1 Electron micrograph of the surface structure of a rose-petal (A). Integrated reflection at a wavelength of 562 nm of CIGS solar cells covered with a flat window and with a rose-inspired window (B) and normalized angular distribution of forward-scattered white-light transmitted through a rose petal replica (C).

The rose petal structure shows further properties which are also beneficial for solar cell application: The transmitted light experiences strong scattering thus elongating its path through the absorber layer. In addition, the highly increased surface area leads to a super-hydrophobic wetting behaviour preventing solar cells from accumulating pollution.

References

[1] Y.-F. Huang, S. Chattopadhyay, Y.-J. Jen, C.-Y. Peng, T.-A. Liu, Y.-K. Hsu, C.-L. Pan, H.-C. Lo, C.-H. Hsu, Y.-H. Chang, C.-S. Lee, K.-H. Chen, and L.-C. Chen, „Improved broadband and quasi-omnidirectional anti-reflection properties with biomimetic silicon nanostructures," Nature nanotechnology ***2***, 770-774 (2007).

[2] J. Woo Leem, X.-Y. Guan, M. Choi, and J. Su Yu, „Broadband and omnidirectional highly-transparent coverglasses coated with biomimetic moth-eye nanopatterned polymer films for solar photovoltaic system applications," Solar Energy Materials and Solar Cells ***134***, 45-53 (2015).

[3] K.-S. Han, J.-H. Shin, W.-Y. Yoon, and H. Lee, „Enhanced performance of solar cells with anti-reflection layer fabricated by nano-imprint lithography," Solar Energy Materials and Solar Cells ***95***, 288-291 (2011).

[4] X. Zhang, Q. Di, F. Zhu, G. Sun, H. Zhang, "Wideband anti-reflective micro/nano dual-scale structures: fabrication and optical properties," Micro & Nano Letters ***6***, 947-950 (2011).

[5] Y. Wang, N. Lu, H. Xu, G. Shi, M. Xu, X. Lin, H. Lin, W. Wang, D. Qi, Y. Lu, and L. Chi, „Biomimetic Corrugated Silicon Nanocone Arrays for Self-Cleaning Antireflection Coatings," Nano Research ***3***, 520-527 (2010).

[6] A. J. Schulte, K. Koch, M. Spaeth, and W. Barthlott, „Biomimetic replicas: Transfer of complex architectures with different optical properties from plant surfaces onto technical materials", Acta Biomaterialia ***5***, 1848-1854 (2009).

Design and Analysis of Holographic Solar Concentrator for semiconductor electrodes for photoelectrochemical hydrogen production device

Rishabh Raj[1*], Sonika Obheroi[1], V Vignesh[3], Rajeev Ranjan[2], R. Navamathavan[3]

[1]*Division of Electronics and Communication Engineering, SENSE, VIT University, Chennai*
[2]*Department of Physics, National Institute of Technology, Jamshedpur, India*
[3]*Division of Physics, School of Advanced Sciences, VIT University, Chennai*
**Corresponding author: rishabh.raj50@gmail.com*

To get rid of storage problem of electricity generated from photovoltaic cells using solar energy, conversion of solar energy into chemical fuel by water splitting is becoming more attractive. Hydrogen is a potential energy carrier that can store and deliver usable energy in absence of sun rays. Research investigations on production of hydrogen by water splitting using solar energy has gained importance due to ease of availability and abundance of both solar energy and water in nature. Photoelectrochemical (PEC) hydrogen production method using semiconductor electrodes is one of the promising methods of hydrogen production from water using solar energy [1]. In PEC system electrodes of semiconducting materials of different band gaps are used. These electrodes absorb solar radiation of suitable wavelength for their efficient working. Semiconductor materials that can accomplish the absorption of light are of different band gaps and hence require different wavelengths of light for their efficient working. Portion of the solar spectrum that does not matches the band gap of the absorber material will degrade the absorber material particularly due to overheating. Therefore, splitting of solar spectrum, filtering out of unwanted portion of solar spectrum and concentrating the desired spectrum on absorber material are highly desirable for semiconducting electrodes in PEC system. Holographic concentrators [2, 3] may perform twin function of spectrum splitting and concentrating specific portion of solar spectrum on absorber material of matched band gap.

In present work dispersing and focusing properties of holographic concentrators has been investigated. Study made on optimization of designing parameters of holographic concentrators to be recorded on high resolution silver halide film and dichromate gelatin films are presented.

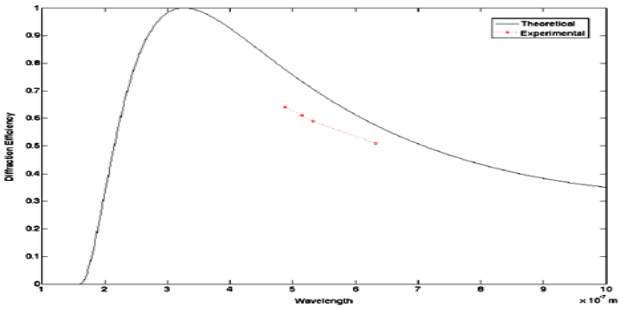

Fig1. *Variation in diffraction efficiency with wavelength for a typically recorded holographic concentrator (n1 = 0.0200, Λ=0.51 μm, n=1.61 and d= 8 μm).*

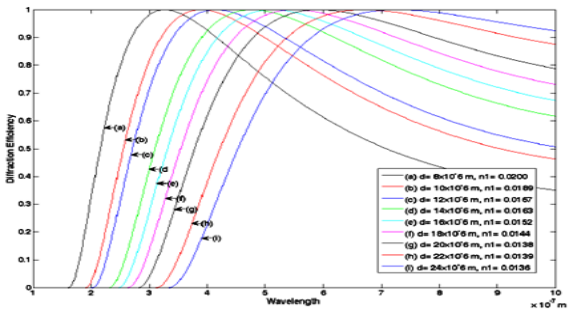

Fig. 2. *Variation in diffraction efficiency with wavelength for different values of film thickness and depth of refractive index modulation at fixed value of Λ=0.51 μm & n=1.61*

To validate the theoretical prediction a comparison of theoretical and experimental variation of diffraction efficiency with wavelength for a typical holographic concentrator recorded on high resolution silver halide film (PFG01) has been done. It is found that holographic concentrator can be used advantageously in PEC system to increase efficiency of hydrogen production by water splitting. It is possible to disperse and focus specific wavelengths on absorber material for their maximum efficiency operation depending upon their band gap. Further, based on theoretical analysis it is also shown that processing parameters of holographic lenses recorded on dichromate gelatin film can be optimized suitably to achieve appreciable diffraction efficiency over desired solar spectrum necessary for absorber materials of different band gap. Unwanted portion of solar spectrum which degrades absorber material and its performance may be filtered out. Experimental result on measured efficiency of a typical holographic concentrators recorded on (PFG01) is very close to theoretical prediction (Fig. 1&2).

References

[1] Walter M G, Warren E L, Mckone J R, Boettchor S W,Mi Q, Santori E A, Lewis N S, Solar Water Splitting Cells.Chemical reviews, 2010; 110: 6446.
[2] Ludman J E.Holographic solar Concentrator. Appl. Opt. 1982; 21: 3057.
[3] Bloss W H, Griesinger M and, Reinhardt E R. Dispersive concentrating systems based on transmission phase holograms for solar applications.Apll. Opt., 1982; 21: 3739.

Near-field photocurrent as characterization tool for graphene devices

Achim Woessner,[1] Pablo Alonso-Gonzalez,[2] Mark B. Lundeberg,[1] Gabriele Navickaite,[1] Yuanda Gao,[3] Qiong Ma,[4] Davide Janner,[1] Kenji Watanabe,[5] Takashi Taniguchi,[5] Valerio Pruneri,[1] Pablo Jarillo-Herrero,[4] James Hone,[3] Rainer Hillenbrand,[6,7] and Frank H.L. Koppens[1]

[1] ICFO - Institut de Ciencies Fotoniques, 08860 Castelldefels (Barcelona), Spain
[2] CIC nanoGUNE, 20018 Donostia-San Sebastian, Spain
[3] Department of Mechanical Engineering, Columbia University, New York, NY 10027, USA
[4] Department of Physics, Massachusetts Institute of Technology, Cambridge, MA 02139, USA
[5] National Institute for Materials Science, 1-1 Namiki, Tsukuba 305-0044, Japan
[6] CIC nanoGUNE and UPV/EHU, 20018 Donostia-San Sebastian, Spain
[7] IKERBASQUE, Basque Foundation for Science, 48011 Bilbao, Spain
***Corresponding author:** achim.woessner@icfo.eu

Graphene is a promising material for optoelectronic applications as its lack of a bandgap leads to a broad band absorption that spans the visible, near-infrared, mid-infrared and THz regime.[1,2] For applications it is of great importance to know the exact optoelectronic properties of the devices used. With common far-field methods the large size of the laser spot after focusing prevents a spatial resolution below the diffraction limit. This leads to smearing of the spatial photocurrent maps, which can mask important details.

Here we introduce a photocurrent measurement technique which is not limited by the diffraction limit. Using a scattering-type scanning near-field optical microscope (s-SNOM) [3,4] with a mid-infrared laser source we excite a strong near-field at the apex of a metallized atomic force microscope probe tip, which acts as a local heat source, generating a temperature gradient in the graphene. This temperature gradient together with a change in Seebeck coefficient leads to a photothermoelectric photocurrent that can be measured spatially. [5]

Here we show how near-field photocurrent measurements with extremely high spatial resolution can be used for characterizing optoelectronic devices made of graphene and graphene heterostructures.[6] We show photocurrent measurements at grain boundaries intrinsic to graphene grown by chemical vapor deposition [7] and extract their polarity. Furthermore we use this unique tool to measure photocurrent from charge puddles [8] of exfoliated graphene on silicon dioxide and show a photocurrent resolution of sub-30 nm. This proofs the extremely high spatial resolution which can be obtained, which ultimately is only limited by the radius of the tip apex. Finally we use the near-field photocurrent technique to confirm the spatial uniformity of the charge neutrality point of graphene encapsulated in hexagon boron nitride.[9] In summary, in this talk we introduce the novel near-field photocurrent mapping technique and show its potential applications in device characterization and quality control.

References

[1] F.H.L. Koppens et al., Nature Nanotechnology, 9 (2014) 780-793.
[2] M. Badioli et al., Nano Letters, 14 (2014) 6374-6381.
[3] J. Chen et al., Nature, 487 (2012) 77–81.
[4] Z. Fei et al., Nature, 487 (2012) 82-85.
[5] N. Gabor et al., Science, 334 (2011) 648-652.
[6] A.K. Geim et al., Nature, 499 (2013) 419-425.
[7] A.W. Cummings et al., Advanced Materials, 30 (2014) 5079-5094.
[8] J. Martin et al., Nature Physics, 4 (2008) 144-148.
[9] L. Wang et al., Science, 342 (2013) 614-617.

Tunable Mach-Zehnder interferometers made from silicon nitride-on-insulator substrates

Anna Ovvyan,[1,*] Uli Lemmer[2], Wolfram Pernice[1]

[1]*Karlsruhe Institute of Technology (KIT), Institute of Nanotechnology (INT), Hermann-von-Helmholtz-Platz 1, 76344 Eggenstein-Leopoldshafen, Germany*
[2]*Karlsruhe Institute of Technology (KIT), Light Technology Institute (LTI), Engesserstrasse 13, 76131 Karlsruhe, Germany*
**Email: anna.ovvyan@kit.edu*

The focus of the work was on the design, modeling, optimization and fabrication of compact low-loss Mach-Zehnder interferometers (MZI) on a silicon nitride-on-insulator platform. Thermo-optical tunability is provided by on-chip microheaters to shift the phase of coherent light in one of the arms of MZI which allows for getting maximum and minimum transmission on desired wavelengths in visible wavelength region.

Thermo-optic MZI switches on SOI were considered previously for applications in the telecoms wavelength region [1,2,3]. Here we realize thermo-optic MZIs which can be used as filter elements integrated in nano-photonic circuits for operation in the visible region. We use low-loss thermo-optic MZI made from silicon nitride. The MZI device consists of spiral waveguides with high packing density in both arms. The waveguides are equipped with meander type microheaters (see Fig. 1) which are written on top of both arms. In contrast to previous work [1,2,3] our scheme makes it possible to double the amplitude of shift of the interference fringes (Fig. 2).

The phase difference at the output of the MZI after heating the longer arm can be expressed as:

$$\Delta\varphi = \Delta\varphi_{fixed} + \varphi_{shift} = \frac{2\pi}{\lambda}\Delta l * n + \frac{2\pi}{\lambda}(l_{spiral} + \Delta l) * \frac{dn}{dT}\Delta T \ ,$$

where λ – is the desired wavelength, Δl – the length difference between the arms, l_{spiral} – the length of spiral waveguide, n – refractive index of SiN, $\frac{dn}{dT} \sim 10^{-5}\ K^{-1}$ – the thermo-optic coefficient of silicon nitride and ΔT - change in the temperature (K).

Due to the fact that the thermo-optic coefficient of silicon nitride is low we employ long spiral waveguides (the length is around 3-6mm) to change the phase $\Delta\varphi$ significantly during heating and hence to increase the shift of the interference fringes.

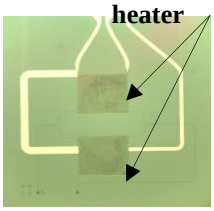

Fig. 1 Optical micrograph of a thermo-optic spiral-arm MZI with meander heaters on top of each arm.

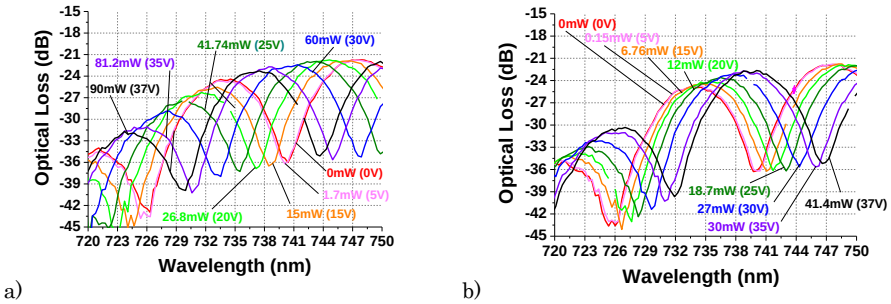

Fig. 2 Optical transmission of a MZI device with a 5.4mm long spiral arm; Different colors represent the shift of the interference fringe under different voltage bias to the meander heater which is on top of the longest arm (a), shortest arm (b).

The fabricated thermo-optic MZI with double spiral geometry feature a compact layout and use dissipated power from the heater more effectively compared with straight-arm MZI. We obtain a shifting power P_π=35-65mW (applied voltage=30-35V) corresponds to a π-phase shift, which shifts the fringe by 6.5nm at the wavelength in the visible region (728nm-740nm) (Fig. 2). We also investigate cascaded thermo-optic spiral-arm MZI (one after another) for improved filter quality.

References

[1] N.C.Harris, Y.Ma, J.Mower, "Efficient, compact and low loss thermo-optic phase shifter in silicon", Optics Express, Vol.22, No. 9, 2014
[2] R.Espinola, M.Tsai, J.Yardley, "Fast and Low-Power Thermooptic Switsch on Thin SOI", IEEE, Vol.15, No. 10, 2003
[3] Q.Fang, J.Song, T.Liow, "Ultralow Power Si Photonics Thermo-Optic Switch With Suspended Phase Arms", IEEE, Vol.23, No. 8, 2011

5.1 W Mid-Infrared Supercontinuum Generation in a Fluoride Fiber from an Actively Q-switched Mode-Locked Tm^{3+}-doped Silica Fiber Laser

Christian Kneis,[1,2] Inka Manek-Hönninger,[2] Thierry Robin,[3] Benoît Cadier,[3] Franck Joulain,[4] Marcel Poulain,[4] Marc Eichhorn,[1] and Christelle Kieleck[1]

[1]*French-German Research Institute of Saint-Louis ISL, 5 rue du Général Cassagnou, 68301 Saint-Louis, France*
[2]*Centre Lasers Intenses et Applications (CELIA), University of Bordeaux - CNRS - CEA - UMR5107, 351 cours de la Libération, 33405 Talence, France*
[3]*iXFiber, Rue Paul Sabatier, 22300 Lannion, France*
[4]*Le Verre Fluoré, Avenue Robert Schuman, 35170 Bruz, France*

***Corresponding author:** christian.kneis@isl.eu*

The generation of mid-infrared (mid-IR) supercontinuum (SC) radiation is intensively investigated owing to the many applications it can be used for, e.g. in spectroscopy, detection systems, spectral fingerprinting or countermeasures [1,2]. Silica fibers cannot be used for mid-IR SC due to their high intrinsic losses in this wavelength range [2]. Therefore, soft-glass materials, which offer transmission in the mid-IR, are mandatory. Fluoride fibers, in particular ZrF_4-BaF_2-LaF_3-AlF_3-NaF (ZBLAN) fibers, are very promising candidates, because they withstand a moderate level of average power, offer transmission in the 2 - 4.5 µm spectral region and have a relative high glass stability [2].

In this research study, a diode-pumped Q-switched mode-locked (QML) thulium (Tm^{3+})-doped double-clad silica fiber laser, emitting around 2 µm, is used to pump a ZrF_4-BaF_2-LaF_3-AlF_3-NaF (ZBLAN) fiber for mid-IR SC generation. The QML regime of the fiber laser is actively generated by two acousto-optic modulators inside the cavity. Wavelength-tunability is enabled by a diffraction grating, used as cavity end mirror of the fiber laser. The performance of the Tm^{3+}- doped fiber laser regarding output power is shown in Figure 1, left.

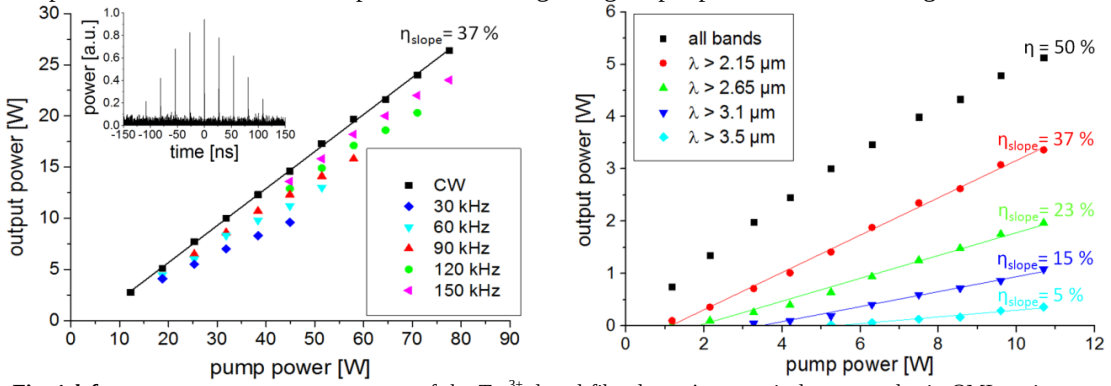

Fig. 1 ***left:*** output power versus pump power of the Tm^{3+}-doped fiber laser, *inset:* typical output pulse in QML regime; ***right:*** SC output power after certain long-wave- pass filters versus pump power.

The Tm^{3+}-fiber laser provided up to 23.5 W (26 W) of average output power in QML (continuous wave) operation with a slope efficiency of 36 % (32 %). The measured beam quality has been close to diffraction-limit. A typical output pulse in QML operation is shown in the inset of Figure 1, left. The system delivered mode-locked pulses with a duration of 7.5 ps, measured with an autocorrelator system, at the fundamentally mode-locked repetition rate of 38 MHz. The Q-switched envelopes had a width between 50 and 150 ns depending on output power level and repetition rate.

A SC output power in all spectral bands of 5.1 W has been achieved with more than 3.4 W/ 2 W/ 1.1 W/ 0.36 W after a long-wave-pass filter with a 3 dB-edge at 2.15 µm/ 2.65 µm/ 3.1 µm/ 3.5 µm resulting in a slope efficiency of 37%/ 23%/ 15%/ 5% (Figure 1, right). A coupling efficiency of 70% into the ZBLAN fiber have been reached via free-space coupling. The spectral power distribution, measured with a monochromator and a liquid nitrogen cooled indium antimonide detector, showed an SC spectrum until the wavelength of 3.7 µm.

References

[1] M. Eckerle, C. Kieleck, J. Swiderski, S. D. Jackson, G. Maze, and M. Eichhorn, "Actively Q-switched and mode-locked Tm^{3+}-doped silicate 2 µm fiber laser for supercontinuum generation in fluoride fiber," Opt. Lett **37**, 512 (2012)
[2] J. Swiderski, and M. Michalska, "High-power supercontinuum generation in a ZBLAN fiber with very efficient power distribution toward the mid-infrared", Opt. Lett. **39**, 910 (2014)

Electromagnetic Simulation of On-chip Optofluidic Devices: liquid core/liquid cladding waveguides

M. Oraie,[1,2,+] H. Latifi,[1,2,*]

[1]*Physics Department, Shahid Beheshti University, Evin, 19839-63113 Tehran, Iran*
[2]*Laser and Plasma Research Institute, Shahid Beheshti University, Evin, 19839-63113 Tehran, Iran*
Corresponding author: latifi@sbu.ac.ir
[+]***Presenting author: m_oraie@sbu.ac.ir***

Optofluidics is a developing field of research emerged from the integration of optical components into Lab-on-a-Chip (LOC) microfluidic devices. Microfluidic devices obey the Navier-Stokes equations [1] which in the time-independent incompressible mode is expressed as:

$$\rho(\mathrm{u}.\nabla)\,\mathrm{u} = \nabla.[-p\,\mathrm{I} + \mu(\nabla\,\mathrm{u} + (\nabla\,\mathrm{u})^T] + \mathrm{F} \tag{1}$$

where ρ is the density, u is the velocity vector, p is pressure and F is the volume force vector. Moreover, we have the time-independent continuity equation written as $\rho\nabla.(\mathrm{u}) = 0$. In order to simulate the behaviour of any time-independent microfluidic system, it is straightforward to solve these equations which provide us with the velocity field and the pressure distribution throughout the microchannel. If we want to analyse the optical properties of the microfluidic channel, we shall know the refractive index profile. The parameters which correlate the optical and fluidic properties are the "concentration" of different species present in the microchannel and their refractive indices. To obtain the concentration profile of each species, we use the following mass balance equations

$$\begin{aligned} \nabla.(-D_i\nabla c_i) + \mathrm{u}.\nabla c_i &= R_i \\ N_i &= -D_i\nabla c_i + \mathrm{u}\,c_i \end{aligned} \tag{2}$$

where c is the concentration of the species, D denotes the diffusion coefficient, R is a reaction rate expression for the species, N is the flux of species and *i* is an index. The velocity vector can be obtained from Eq. (1) and be inserted in equation (2) to find the concentration profile. The next step is to use the concentration profile of the microfluidic channel to find the refractive index profile. In this study, we suggest to employ the Effective Medium Theory of Bruggeman which gives the effective optical (or electrical) properties of a mixed media based on the refractive index and volume filling fraction of its constituents. This theory can be expressed as:

$$\sum_i f_i \left\{ (n_i^2 - n^2)/(n_i^2 + 2n^2) \right\} = 0 \tag{3}$$

where f_i denotes the volume filling fraction of ith species, n_i their refractive indices and n the effective refractive index.

By implementing Eq. (3) the profile index of microfluidic channel can be obtained and, then, by using Maxwell's equation, the optical properties of a microfluidic channel can be extracted. As an example, we have carried out this procedure to analyse the liquid core/liquid cladding (L^2) optofluidic waveguide [2]. As it is shown in Fig. 1.c the z-component of electric field is confined within the core region where the refractive index is higher.

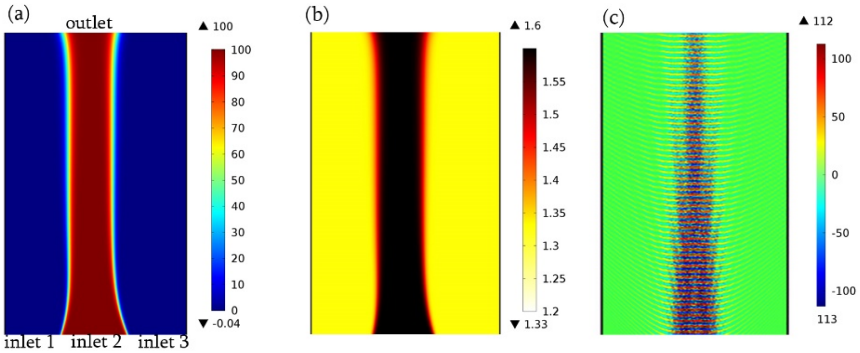

Fig. 1. Optical and fluidic properties of a L^2 waveguide (the cladding liquid is injected via inlets 1 and 3 and the core liquid is injected via inlet 2 and all of them exit from the outlet) **:**(a) the concentration profile of the core liquid (mol/m^3), (b) the Refractive index profile throughout the channel (c) the z-component of electric field (V/m) confined inside the core liquid.

References

[1] H. Bruus, *Theoretical Microfluidics*, (Oxford University Press, Oxford, 2008).
[2] D. B. Wolfe, R. S. Conroy, P. Garstecki, B. T. Mayers, M. a Fischbach, K. E. Paul, M. Prentiss and G. M. Whitesides, "Dynamic control of liquid-core/liquid-cladding optical waveguides.," Proc. Natl. Acad. Sci. U. S. A. , **101**,12434–12438 (2004).

Study of scintillating fibers optical properties

Rodnova Z.,[1] Lazarev V.,[1] Leonov S.,[1] Dvoretskiy D.,[1] Karasik V.[1]

[1]Bauman Moscow State Technical University, 105005, 2nd Baumanskaya, Moscow, Russia
***Corresponding author:** zhannarodnova@gmail.com*

Detectors based on scintillating plastic light guides have recently become quite widespread in elementary particle physics. Such detectors enable to detect scattered protons and electrons trajectories and measure collider luminosity at the point where particles collide [1]. With the help of scintillating counters energy spectra of electrons and gamma rays can be measured [2].

The scintillation detector working principle is based on the fluorescent properties of certain materials that show when the material interacts with particles or with radiation. Such materials are called scintillators. Registering the fluorescent radiation with the help of a photodetector and analyzing it can obtain data about the particle or about the radiation interacting with the plastic fiber light guide.

Scintillator detectors based on plastic fiber light guides are widely used nowadays, and they all have a common constructive feature connected with the vertical handling of the light guide. This fixation method leads to extension caused by the light guides' own weight, which leads to additional optical losses and possible reduction of the scintillator transmission [3].

The goal of this work is attenuation measurement in scintillating fiber light guides and the examination of the relation between the light guide deformation and its loss. An experimental setup for plastic fiber light guide loss measurement is proposed, plastic light guide loss measurements are conducted, and the relation between the losses and the deformation is established.

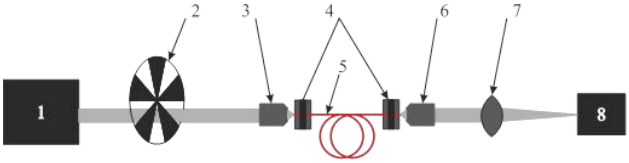

Fig. 1 Experimental setup for measuring the losses in the light guide (1 – white laser with an acoustic-optical filter; 2 – modulator; 3 – input lens (10x); 4 – points of fiber adjustment; 5 – the measured light guide; 6 – output lens; 7 – focusing lens; 8 – detector)

The experimental results are shown on Figure 2.

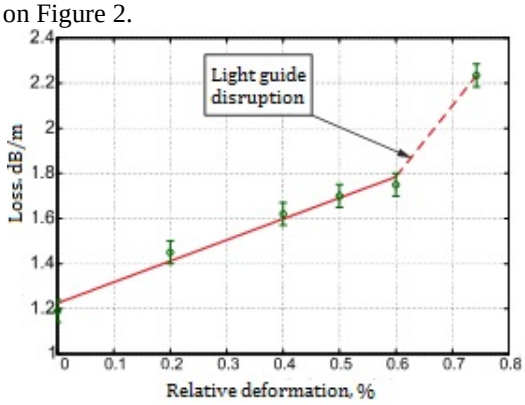

Fig. 2 The light guide loss to deformation ratio

The experiments have shown that a 0,2% deformation (in a light guide 1,75 m long with a 3,5 mm extension) the losses in a scintillating light guide were 1,4 dB/m. On the brink of disruption (0,6% deformation) losses increase to 1,8 dB/m. The graph shows the loss to deformation relation is linear.

The data obtained has to be considered when handling light guides, especially when calculating elementary particles detectors' sensitivity based on scintillating light guides.

References

[1] Mapelli A. Scintillation Particle Detectors Based on Plastic Optical Fibres and Microfluidics : thesis for obtaining D.Sc., Lausanne, 2011.
[2] Bisplinghoff J. [et al.] A scintillating fibre hodoscope for high rate applications // Nuclear Instruments and Methods in Physics Research A. 2002. № 490. P. 101–111.
[3] Radiation damage on Kuraray SCSF-78M and SCSF-78MJ fibers: literature study, September 2012 / LHC. Lausanne : LHC, 2012. 15 p.

Random Telegraph Signal vs Random Binary Sequence for Suppressing the Stimulated Brillouin Backscattering

Mehdi Alem*, Marcelo A. Soto, and Luc Thévenaz

EPFL Swiss Federal Institute of Technology, Institute of Electrical Engineering
SCI STI LT, Station 11, CH-1015 Lausanne, Switzerland
**Corresponding author: mehdi.alem@epfl.ch*

Launching constant-intensity light waves or long duration optical pulses into optical fibers is indispensable in a variety of applications such as fiber lasers and amplifiers, fiber-optic parametric devices, and optical fiber sensing. In such continuous wave (CW) or quasi-CW optical systems, stimulated Brillouin scattering (SBS) is the most detrimental nonlinear effect. The SBS process couples acoustic phonons to the photons of the forward traveling optical field and backward scattering Stokes lightwave through a phase-matched third-order nonlinear interaction [1]. As the peak power of an optical pump launched into the fiber increases, SBS enhances dramatically the acoustic wave that couples the optical power from the forward lightwave into a reflected one with a lower frequency reduced by ~11 GHz; this way the pump power drastically depletes. Due to the rather long phonon lifetime of ~5 ns, the SBS is a narrow linewidth process that requires a highly coherent light and thus can be substantially suppressed by broadening the optical pump spectrum via modulation.

The effective SBS gain spectrum resulting from the modulated light is given by the convolution of the Lorentzian gain and the normalized power spectral density (PSD) of the modulated pump $S(f)$ as follows [2].

$$g(f) = \frac{g_{\mathrm{B}}}{1 + 4\left(\frac{f}{f_{\mathrm{FWHM}}}\right)^2} \otimes S(f), \tag{1}$$

in which $g_{\mathrm{B}} = 3 \times 10^{-11}$ m/W is the maximum Brillouin gain, $f_{\mathrm{FWHM}} = 30$ MHz is the Brillouin full width at half maximum (FWHM) bandwidth, and $\otimes$ denotes the convolution operation. In order to keep the intensity of light fixed it is necessary to use phase or frequency modulation. A very common way to do so is through an electro-optical phase modulator driven by a pseudo-random binary sequence (PRBS) which applies 0 and π phase shift to the optical field [3]. The performance limit of PRBS with a bit duration of T is given by a complete random binary sequence (RBS) shown in Fig.1 (a) with spectrum $S_{\mathrm{RBS}}(f) = T\mathrm{sinc}^2(Tf)$ [4].

Instead of using random phase shift, a novel approach to phase modulation is a random pulse width modulation of consecutive 0 and π phase shift with an average bit duration of T. Although there are many possibilities for the probability distribution of the pulse width, an exponential distribution of $e^{-t/T}$ with mean T is chosen since the process is theoretically memoryless and it can be practically implemented using a weak laser beam and a single-photon detector connected to a flip-flop switch. The signal produced this way is called the random telegraph signal (RTS), shown in Fig.1 (b), with the spectrum $S_{\mathrm{RTS}}(f) = T/(1 + (\pi T f)^2)$ [5]. Fig.1 (c) depicts the normalized Brillouin gain spectrum given in Eq. (1) for three cases, no modulation, RBS-modulation and RTS-modulation. It is evident that by using modulation the peak gain decreases and so the threshold power increases. Therefore, the RTS can give higher threshold compared to the RBS and thus any PRBS modulations.

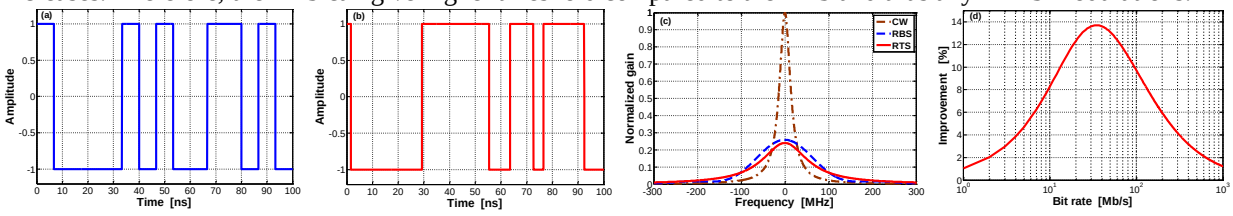

Fig. 1 The modulating pulse sequences (a) RBS and (b) RTS for 150 Mb/s; Brillouin gain spectrum (c) in three cases: unmodulated, RBS-modulated, and RTS-modulated with 150 Mb/s; (d) the improvement percentage of the threshold power using RTS instead of RBS versus the bit rate.

The improvement behavior of using the RTS for suppressing the SBS compared to the RBS versus the modulation bit rate is shown in Fig.1 (d). The vertical axis indicates the increase in the SBS threshold power achieved using the RTS instead of the RBS. As it is clear, for typical values of bit rate the proposed RTS signal acts better than the RBS and the optimal bit rate in which there is almost 14% improvement is close to the Brillouin bandwidth. Moreover, in the used range of 100-200 Mb/s the threshold increases by more than 6%.

References

[1] C. Zeringue, I. Dajani, S. Naderi, G. T. Moore, and C. Robin, "A theoretical study of transient stimulated Brillouin scattering in optical fibers seeded with phase-modulated light," Opt. Express **20**(19), 21196-21213 (2012).

[2] M. González Herráez, K. Y. Song, and L. Thévenaz, "Arbitrary-bandwidth Brillouin slow light in optical fibers," Opt. Express **14**(4), 1395-1400 (2006).

[3] A. Flores, C. Robin, A. Lanari, and I. Dajani, "Pseudo-random binary sequence phase modulation for narrow linewidth, kilowatt, monolithic fiber amplifiers," Opt. Express **22**(15), 17735-17744 (2014).

[4] J. G. Proakis and M. Salehi, *Digital Communications*, 5th ed. (McGraw-Hill, 2007).

[5] A. Papoulis, *Probability, Random Variables and Stochastic Processes*, 3rd ed. (McGraw-Hill, 1991).

Next Generation Optical Access Networks: Technologies and Economics

Ali Shahpari

Department of Electronics, Telecommunications and Informatics, University of Aveiro and Instituto de Telecomunicações, Campus Universitário de Santiago, 3810-193 Aveiro, Portugal
***Corresponding author:** Ali@ua.pt*

Due to the plurality of end user types and very heterogeneous nature of services, Internet data traffic in access network is becoming very dynamic and unpredictable. This makes the design of future optical access networks challenging. From cost point of view, complexity of the cost sensitive elements should be reduced, eventually by (i) keeping Optical Distribution Network (ODN) in Point-to-Multi Point (PtMP) and unchanged for as much time as possible, (ii) reducing complexity, cost and energy consumption per bit at each part of the network, especially in the customer side and (iii) increasing barriers to providers change. From the value point of view, client's satisfaction is a key that can be achieved by (i) investing in a good technology from the first day, (ii) pay as you grow approach with enough flexibility to keep up surprising the client, (iii) innovation in the service and providing fast reaction to the markets. From what was referred, state-of-the-art optical access networks rely on both a large network capacity and scalability, together with flexible and efficient usage of spectral resources, easy maintenance, and coexistence with other existing access networks and video overlay, as shown in Fig. 1.1. In addition, extended reach is a key requirement to increase coverage area and reduce costs and energy per user.
Passive Optical Networks (PONs) are stemming as balanced alternatives for deploying the next generation future proof broadband. Technologically, several possibilities for PONs that offer efficient usage of bandwidth and energy per bit are being considered nowadays. Coherent based PON is envisioned to be as one of the promising candidates for Next Generation Optical Access Networks (NG-OAN). Clearly, this technology still requires maturing in order to meet the price targets for access networks as well as to meet the type of services and working conditions (rate, reach, energy consumption, dedicated/shared bandwidth) [1]. This work starts by addressing some of the factors that can be considered in the energy efficiency and resources optimization of optical access networks. Then it continues to investigate in detail the novel spectrally efficient coherent PON.

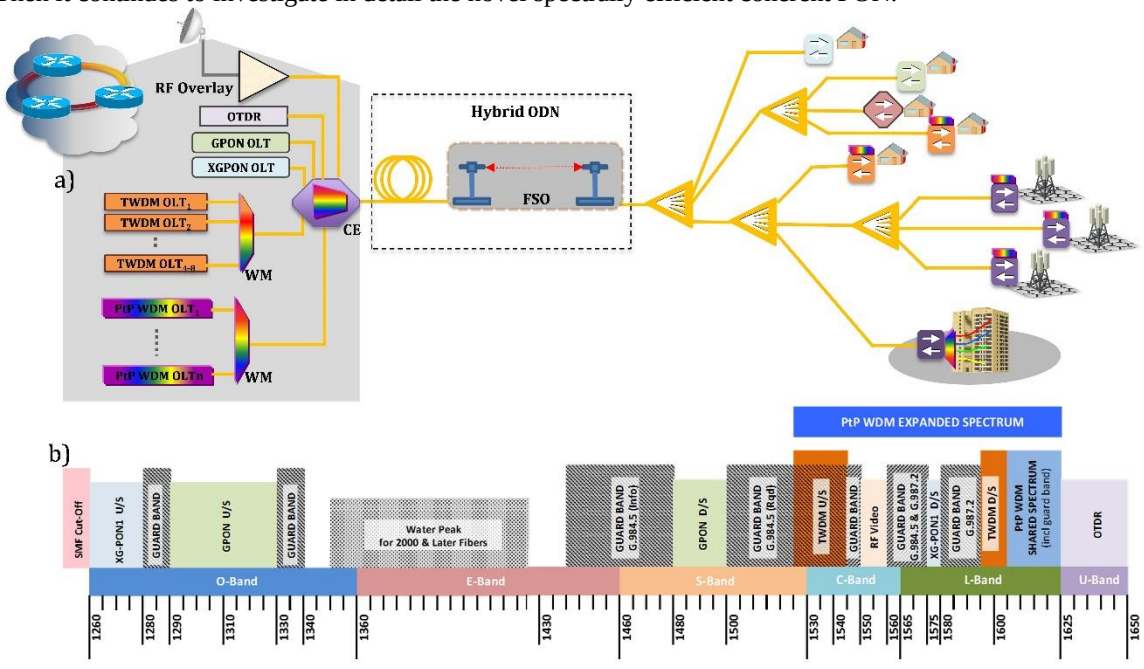

Figure 1 (a) Multiple system configuration for next generation optical access networks, (b) wavelength plan and coexistence representation [2]. CE: Co-existence Element, WM: Wavelength Mux (demux), FSO: Free Space Optics.

References

[1] A. Shahpari, J. D. Reis, R. Ferreira, D. Neves, M. Lima and A. Teixeira, "Terabit+ (192 x 10 Gb/s) Nyquist shaped UDWDM coherent PON with upstream and downstream over a 12.8 nm band," Proc. Optical Fiber Communication Conf. (OFC), Anaheim, CA , March 2013, paper PDP5B.3. Citation 35.

[2] ITU-T recommendation G.989.2 (draft), "40-Gigabit-capable passive optical networks: Physical media dependent layer specification," April 2014.

Optical vortex response due to specified phase disturbance

Mateusz Szatkowski,[1] Agnieszka Popiołek-Masajada,[1] Jan Masajada,[1]

[1]*Department of Optics and Photonics, Faculty of Fundamental Problems of Technology, Wroclaw University of Technology, Wyb. Wyspianskiego 27, 50-370 Wroclaw, Poland*
***Corresponding author:** mat.szatkowski@gmail.com*

Optical Vortex Scanning Microscope (OVSM) uses focused laser beam with an optical vortex to scan the sample. The current setup of the OVSM was presented in [1]. The setup is based on the carrier frequency interferometry. Optical vortex is generated by spiral phase plate (vortex lens). The optical vortex can be moved inside the focused light spot by shifting the vortex lens [2, 3]. The range of this movement in the observation plane is reduced comparing to the range of the vortex lens shift. Thus, we have a precise way for sample scanning. This new scanning method was tested experimentally with simple phase micro-objects. It was shown that our system is sensitive to small phase disturbances which have an impact on both optical vortex position and phase profile

One of the challenges for the OVSM is finding the effective procedures for surface topography reconstruction. We proposed an experimental setup shown in (Fig. 1) to support the works focused on this problem. The Spatial Light Modulator (SLM) is used as an object. SLM allows generating any phase disturbance with specified value and size. The SLM is illuminated by the vortex beam (beam carrying optical vortex). Our system gives an opportunity to measure optical vortex response due to phase modifications introduced by the SLM. We measured optical vortex reaction to simple objects generated by SLM, especially by changing object position and its phase value. Phase retrieval algorithm and results of these experiments will be presented. These results show the way in which the OVSM should be developed.

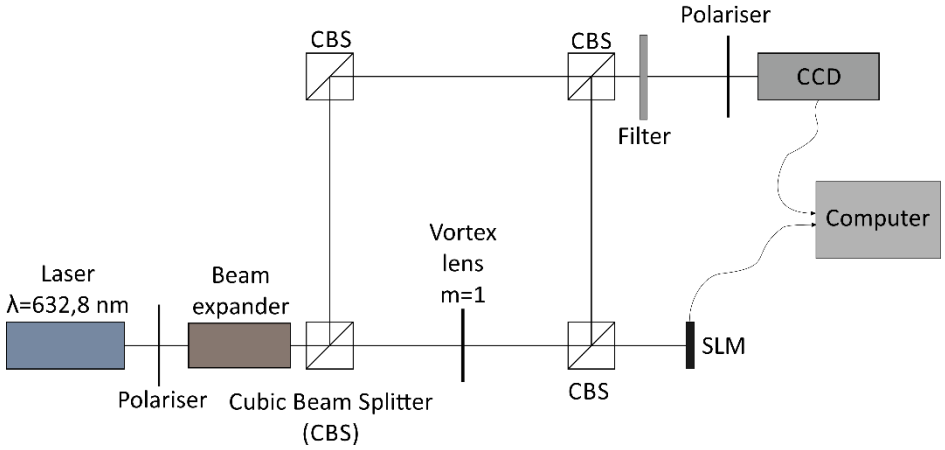

Fig. 1 Setup for measuring optical vortex response due to specified phase disturbance. SLM is used as an object. SLM introduces phase modification into the beam which is carrying the optical vortex generated by vortex lens.

[1] Augustyniak, J., Popiołek-Masajada, A., Masajada, J., Drobczyński, S., "News scanning technique for the optical vortex microscope", Appl, Oot, **51**, C117-C124 (2012).
[2] Masajada, J., Augustyniak, I., Popiołek-Masajada, A., "Optical vortex dynamics induced by vortex lens shift – optical system error analysis", J. Opt., **15** 044031 (2013).
[3] Masajada, J., Leniec, M., Augustyniak, I., "Optical vortex scanning inside the Gaussian beam", J. Opt. **13** 03571 (2011).

Core/Shell/Quasi-Shell Quantum Dot Absorbers: A Dual Sensitization Strategy for High Performance Photovoltaics

Atharva Sahasrabudhe, Dr. Sayan Bhattacharyya

Department of Chemical Sciences, Indian Institute of Science Education and Research (IISER) Kolkata, Mohanpur - 741246, India

Corresponding author: sayanb@iiserkol.ac.in

.

The current challenges,[1,2] in designing highly efficient quantum dot sensitized solar cells (QDSCs) are (i) expanding the light-harvesting range; (ii) improving charge separation and (iii) suppressing interfacial charge recombination at the TiO_2/quantum dot/electrolyte interface. Type-II quantum confined semiconductor heterostructures as sensitizers offer a unique way to address these issues, since the exciplex state of the type-II system widens the light absorption window while the staggered juxtaposition of the conduction and valence bands drives charge separation in such systems through compartmentalization of electrons and holes,[3]. This dissertation presents an optimized dual sensitization strategy for high performance, *all-aqueous* processed liquid junction QDSCs. Particularly, type-II core/shell/*quasi-shell* CdTe/CdS/*CdS* quantum dots (QDs) were used as absorbers and the QDSCs were fabricated by a 2 step approach which comprises of: (a) CdTe/CdS core/shell QD self assembly on porous TiO_2; (b) Deposition of an additional CdS layer through successive ionic layer adsorption and reaction (SILAR). At first, the QD surface coverage was optimized by systematic pH variation, whereby the device efficiency was improved from 2.04($\pm$0.01) % (pH 11) to 3.696($\pm$0.005) % (pH 13). Secondly, the individual roles of the shell and the *quasi-shell* and their overall synergistic effect on device performance were critically analyzed. Various charge transport and recombination measurements revealed that while the epitaxial shell passivated the core surface traps, the non-epitaxial *quasi-shell* passivated the TiO_2 surface states and hence the two acted in tandem to increase the overall device performance. Thus while the conversion efficiency (η) was 1.45($\pm$0.10) % and 3.62($\pm$0.40) % for core/shell and core/*quasi-shell* sensitized devices respectively, it reached an impressive 5.69($\pm$0.02) % with core/shell/quasi-shell architecture (Fig. 1). Furthermore, the device performance was found to be extremely sensitive to the *quasi-shell* thickness. The origin of such dependence was traced back to increased interfacial recombination rate using various dynamical techniques such as impedance spectroscopy, open-circuit voltage decay and dark current measurements,[4]. While the light harvesting efficiency kept on increasing, the overall device performance dropped after a critical *quasi-shell* thickness (4 SILAR cycles), which highlights the detrimental effect of QD overloading on the device output (Fig. 2). Having rationally optimized and established the roles of different components, the modified deposition technique allowed us to fabricate liquid junction devices with efficiencies as high as 6.41% (J_{sc} = 20.32 mA/cm^2, V_{oc} = 0.61 V, FF= 51%) (champion cell) which, notably, is the highest for any *all-aqueous* processed QDSC.

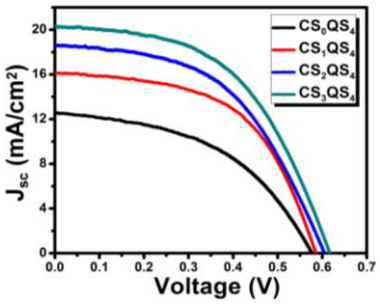

Fig. 1. Shell thickness dependant device performance.

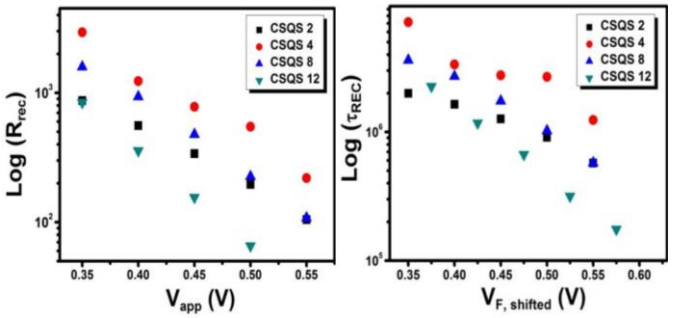

Fig. 2 Effect of quasi-shell thickness on (left) recombination resistance and (right) recombination lifetime.

References

[1] Kamat, P. V. "Quantum Dot Solar Cells. The Next Big Thing in Photovoltaics" J. Phys. Chem. Lett,, ***4***, 908– 918 (2013)
[2] Albero, J.; Clifford, J. N.; Palomares, E."Quantum Dot Based Molecular Solar Cells" Coord. Chem. Rev., ***263***, 53– 64 (2014**)**
[3] Kamat, P. V."Quantum Dot Solar Cells. Semiconductor Nanocrystals as Light Harvesters" J. Phys. Chem. C, ***112***, 18737– 18753 (2008**)**
[4] Gonzalez-Pedro, V.; Xu, X.; Mora-Sero, I.; Bisquert, J ".Modeling High-Efficiency Quantum Dot Sensitized Solar Cells" ACS Nano, ***4***, 5783– 5790 (2010)

Use mechanisms of the Holographic Interferometry in Sciences of Visual Arts: analytical theoretical study

Ahmedien. Diaa Ahmed Mohamed

Graduated School of Arts, University of Bern, 15 Waldmannstrasse (3027, Bern, Switzerland)
***Corresponding author:** diaa.ahmedien@gmail.com*

This paper focuses on some of the advanced holography uses, including their scientific concepts and techniques, but via relatively different aspect about that usually is used for scientific purposes. Current holographic scientific developments in sciences of visual arts will be discussed in this research. According to sciences of visual arts, three main holographic mechanisms have been classified in this research: laser interferometry, holographic recording (analog & digital) and holographic stereogram that are used in installation art, simulation art and real time art, respectively.

Three major questions could be answered through this research: To what extent can holographic mechanisms be similarly used in both of optics sciences and processes in sciences of visual arts? Can sciences of visual arts translate the scientific principles and concepts of holographic interferometry theoretically and practically? What is the nature of the contribution that can be provided by both of optics science and sciences of visual arts to enhance the practical holographic techniques? this analytical study aimed to design analytical descriptive diagram that can illustrate and compare the progression steps between holographic techniques and their usage in visual arts processes via two parallel lines, through documenting some of the leading examples in visual arts that have not only proven the depth of laser applications but also achieved considerable shifts in some of artistic trends and the natural of creation processes in visual innovative works, where the optics labs became studios for artists, which usually prefer show their scientific artworks in public space and that is why some of complicated scientific techniques became well known in public communities.

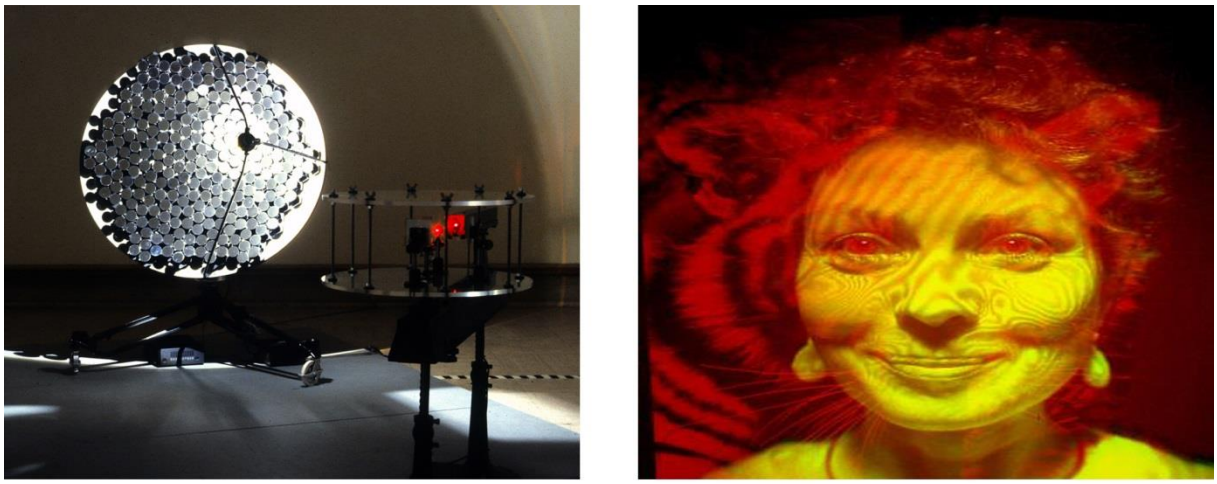

Fig. 1 Two leading examples of holographic interferometry and analog holography recording, A: Shawn Brixy, Celestial Vaulting, 1990, Ohio, USA. B: Margaret Benyon, TiGirl, 1985, Victoria & Albert Museum, London.

In his installation entitled Celestial Vaulting fig1.A, Brixy was aiming to create a holographic interferometry installation that uses real-time optical laser holography to determine the minute time-of-flight difference between phases entangled photons at the speed of light, while In Benyon's portrait, holographic patterns on the face of the artist are combined with the stripes on a tiger's head, a vertical strip dividing the tiger's mask aligns both animal and human eyes, to create a haunting image. The light and dark patterns are produced by putting the pulsed laser into "double-pulse" mode.

References

[1] J. Elkins, *Theorizing Visual Studies*, First Edition (Taylor & Francis, London, 2011)
[2] O. Herwing, T. Thallemer, *Unity of Art and Science*, First Edition (ARNOLD SCHEN, USA, 2013)
[3] R. Ascotte, *Art, Technology and consciousness*, First Edition (ITELLECT, Bristol, 2005)
[4] S. Wilson, *Art and Science Now*, First Edition, (Thames & Hudson, UK, 2012)

Direct Laser Writing of Volume Fresnel Zone Plates in Silicon

Ahmet Turnali[1]*, Onur Tokel[2], Ihor Pavlov[2] and F. Ömer Ilday[1,2]

[1] *Department of Electrical and Electronics Engineering, Bilkent University, 06800 Ankara, Turkey*
[2] *Department of Physics, Bilkent University, 06800 Ankara, Turkey*
* ***Corresponding author:*** *turnali@ee.bilkent.edu.tr*

Functional optical elements fabricated on silicon (Si) constitute fundamental building blocks of Si photonics [1]. For the fabrication of these elements, conventional lithography and etching techniques are used. In spite of the success of these techniques, a functional optical element embedded *inside* silicon simply does not exist. Here, we present a maskless, one-step laser writing technique for creating phase-type Fresnel zone plates in the bulk of Si. Due to their effectiveness over a broad spectra, Fresnel zone plates (FZPs) are widely used in various micro-imaging applications [2]. Similar lenses have been fabricated inside silica [3,4], but are limited to the transparency window of silica. The silicon counterpart of these elements have been impossible to fabricate so far. By exploiting nonlinear absorption within the focal volume of a tightly focused laser, we generated permanent refractive index changes in Si. The imprinted high-index contrast was then used to fabricate a FZP inside Si. This three dimensional (3D) method can allow for alignment-free multilens systems. Moreover, using silicon as the lens material is fully CMOS compatible and applicable to silicon integrated optics, including single and array detectors.

Fig. 1(a) shows the experimental setup. We used a home-built, all-fibre master oscillator power amplifier (MOPA) system that produces 5.5 ns pulses at 150 kHz repetition rate. During the writing we used 3.3 W of average power, at 1.55 μm, where silicon is transparent. A three-axis motorised stage was used to precisely position the sample with respect to the laser focus. The designed FZP has 20 zones corresponding to a focal length of 25 cm in Si. This translated to a focal length of 7.24 cm in air.

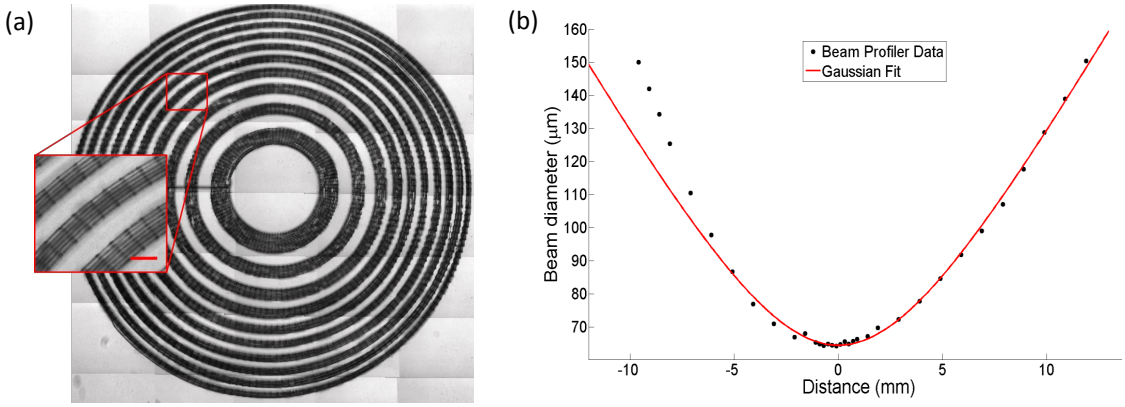

Fig. 1 (a) Infrared microscope image of the laser-written phase-type Fresnel zone plate. Dark zones correspond to the processed areas. The outermost zone radius is 1.5 mm. Scale bar indicates 70μm (b) Focused laser beam diameter as a function of relative position. The beam profiler data (black) is fitted with a focused gaussian (M^2 = 1.46) shown with the curve in red.

For the fabrication of the lens, only even-numbered zones are processed, while odd-numbered zones were left untouched. This is modelled as a two-step refractive index distribution. The concentric zones are defined by the radial positions, as $r_n = \sqrt{n\lambda f + (n\lambda/2)^2}$, where r_n indicates the n^{th} Fresnel zone's radius. To create an effectively fully processed zone, we created concentric circles with 10 μm separation in the even numbered zones. Modification energy was kept at 22 μJ/pulse and the radial translation speed was at $\sim$ 0.2 mm/sec. Fig. 1(b) shows an IR microscope image of the lens. Characterisation of the lens and focal point measurements were done with a beam profiler. Focal point was measured at 7.3 cm away from the lens for incident beam of 3 mm diameter. This value is in good agreement with the 7.24 cm calculated value. Beam quality of the focused beam was measured to be M^2 = 1.46 (Fig. 1(c)).

In conclusion, a 3D phase-type FZP in the bulk of silicon was designed and fabricated by using a high-power pulsed infrared laser. This is the first optical element fabricated inside the bulk of silicon to our knowledge. Notably, the FZPs can be used in near-IR imaging applications.

References

[1] J. Leuthold, C. Koos and W. Freude, "Nonlinear silicon photonics," Nature Photon. **4**, 535 (2010).
[2] T. Grulois, G. Druart, N. Guerineau, A. Crastes, H. Sauer and P. Chavel, "Extra-thin infrared camera for low-cost surveillance applications," Opt. Lett. **39**, 3169 (2014).
[3] E. Bricchi, J. D. Mills, P. G. Kazansky and B. G. Klappauf, "Birefringent Fresnel Zone Plates in Silica Fabricated by femtosecond laser machining," Opt. Lett. **27**, 2200 (2002).
[4] P. Srisungsitthisunti, O. K. Ersoy and X. Xu, "Volume Fresnel zone plates fabricated by femtosecond laser direct writing," Appl. Phys. Lett. **90**, 011104 (2007).

Single pulse ultrafast laser sub-micron ablation of graphene

A. Gil Villalba*, C. Xie, R. Salut, L. Furfaro, R. Giust, J. M. Dudley, F. Courvoisier
1. Institut FEMTO-ST, UMR 6174 CNRS University of Franche-Comte, 25030 Besançon Cedex, France

****Corresponding author:** abel.gilvillalba@femto-st.fr*

Graphene nanopatterning has a very wide range of applications for next generation technology: photonics, displays and solar energy [1]. Femtosecond laser ablation is extremely advantageous for large scale patterning because it is a fast reconfigurable, high throughput, processing technology useable on non-flat surfaces. Previous studies of fs-laser ablation patterning in accumulative thermal regime (burning) have shown high accuracy (down to <100 nm) but it is a slow process [2]. Single shot femtosecond pulse ablation experiments were recently carried out on graphene but only at scales larger than typ. 1μm [3,4]. To decrease the range of processed size, accurate measurement of ablation threshold was needed.
With a novel technique for single shot ablation threshold measurement, we have surprisingly observed a strong deviation from the ablation threshold model for single layer graphene. When the processed structures have a transverse size below 800 nm, the ablation probability decayed with the beam diameter size.
Our new measurement technique is based on matching SEM image of the damage produced with well calibrated beam image. To gain high accuracy, the beam is internally structured (honeycomb-like) with several regions generating small and large diameter beam features in the range ~0.4-3 μm. Figure 1 shows an example of correspondence. In addition, we choose a non-diffracting beam, avoiding errors arising from beam to sample positioning at high numerical aperture [4]. While the measurement of ablation threshold is usually performed by a fit over a range of ablation crater diameters, our new approach allows us to measure the ablation threshold for a single structure. For the range over 1 μm diameter, the single shot ablation fluence threshold of CVD monolayer graphene was determined for pulse durations of 130 fs, 1 ps and 3 ps, and the threshold values were respectively 139 mJ/cm2, 166 mJ/cm2 and 190 mJ/cm2 (+/- 8mJ/cm2 error bar for each).

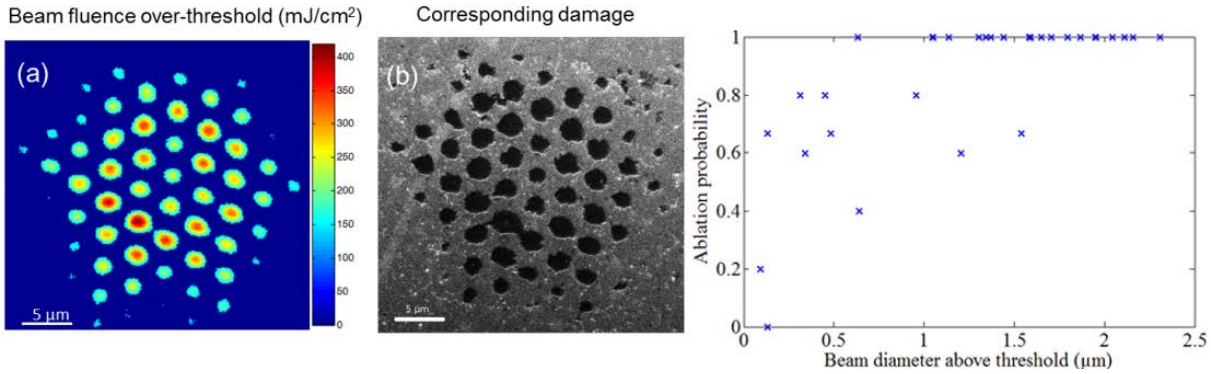

Fig. 1 Comparison of fluence distribution (a) with damage (b) for a given intensity distribution, pulse duration (130 fs) and input pulse energy (1.3 μJ). In (c) we show the probability of ablation in a disk as a function of the energy contained in it.

We observe that, for beam sub-structures with sizes below 800 nm, ablation probability decreases with the beam size whereas ablation was expected from the laser intensity distribution. Figure 1(c) shows the ablation probability vs the beam diameter in the region exceeding the ablation threshold. Several reasons arising from the material properties can explain this deviation for graphene and will be discussed [5]. Our approach opens new perspectives for modelling and controlling materials processing by ultrashort laser pulses**.**

References

[1] F. Bonaccorso, Z. Sun, T. Hasan, and A. C. Ferrari,"Graphene Photonics and Optoelectronics" Nature Photon.**4**,611–622 (2010).

[2] R. J. Stohr, R. Kolesov, K. Xia, and J. Wrachtrup, "All Optical High-Resolution Nanopatterning and 3D suspending of Graphene "ACS Nano**5**, 5141(2011).

[3] J-H.Yoo, J.B. In, J.P. Park, H. Jeon, and C.P. Grigoropoulos,"Graphene folds by femtosecond laser ablation", App. Phys. Lett.**100**, 233124(2012).

[4] B. Wetzel et al, "Femtosecond laser fabrication of micro and nano-disks in single layer graphene using vortex Bessel beams", Appl. Phys. Lett. **103**,241111 (2013).

[5] S. Martin, A. Hertwig, M. Lenzner, J. Krüger, W. Kautek, " Spot-size dependence of the ablation threshold in dielectrics for femtosecond laser pulses ", Appl. Phys. A **77**, 883 (2003).

Micro-channel machining using high-energy femtosecond Bessel beams

Sambit Mitra[1,2], Margaux Chanal[1], Raphaël Clady[1], Alexandros Mouskeftaras[1], David Grojo*[,1]

[1]Aix-Marseille University, CNRS, LP3 UMR 7341, F-13288
[2]Karlsruhe Institute of Technology, 76131 Karlsruhe, Germany
***Corresponding author:** grojo@lp3.univ-mrs.fr*

The use of laser in material processing has gained great importance over other methods primarily due to its capability of material modifications in a highly precise manner. The main parameters which are important for such processing like the beam profile, energy, interaction times etc. can be easily varied depending on its usage [1]. Two such parameters that are of primary importance in our experiment are the interaction time and beam profile. We irradiate the material with femtosecond pulses to induce optical breakdown in the material. A process by which materials can undergo a phase or structural modification, leaving behind a localized permanent change in the refractive index of even a void [2]. To ensure controllable bulk modification, the wavelengths chosen are transparent to the material, and affect it only inside the focal volume, where the intensity is high enough to induce multi photon ionization.

A Bessel beam, as the name suggests, is a beam whose electric field distribution is accurately defined by a zero-order Bessel function of the first kind (J_0) [3]. A specificity of Bessel beam is that they have a focal volume with the shape of an ultra-high aspect ratio channel which can be used to damage the material with a single pulse shot. Our presentation reports on details of a functional experimental design for Bessel beam generation, capable of handling ultrashort pulses of very high energy (up to 1.2mJ) at pulse durations of 50fs. We use an axicon based method to produce the Bessel beam with minimum intensity loss. A setup using such high energy ultrashort pulses for Bessel beam generation is not present in literature and it allows us to deliver intensities exceeding the breakdown threshold for air or any dielectric, along controlled channels, with lengths exceeding 5 mm. Our experiment is developed at 1300 nm, to avoid pulse broadening by dispersion in the optical components. In addition, this long wavelength allows us to envision deep machining experiment in narrow gap materials (e.g. semiconductors) [4]. This proposed design represents a significant up-scaling of recent high-aspect ratio machining experiments [5]. We produce micro-channels through glass substrates using single-shot femtosecond pulses. We conclude that aspect ratios exceeding 1:1000 can be achieved.

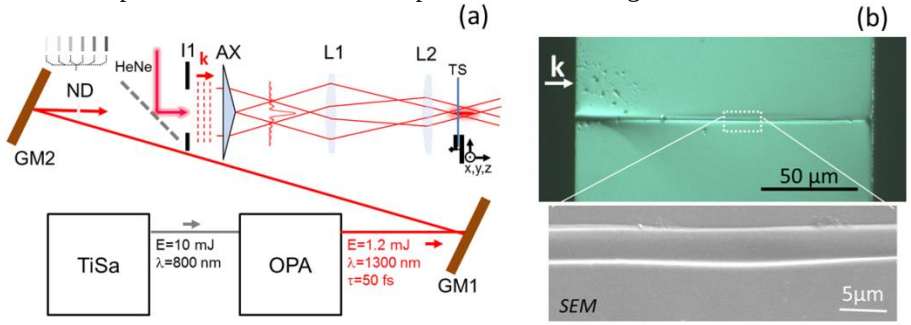

Fig. 1: (color online) (a) Experimental arrangement to produce and perform micromachining experiments with high energy femtosecond Bessel beams. The target substrates (TS) are mounted on a XYZ motorized stage. TiSa is a Ti:sapphire femtosecond laser delivering pulses of 10 mJ to pump an optical parametric amplifier for wavelength conversion at 1300 nm. Neutral density filters (ND) are used to control the energy. Two irises (I1 and I2), a cw HeNe laser and two gold mirrors are used to perform the alignments. The high intensity Bessel beam is generated using a modest angle axicon (AX) and a 4-f arrangement with two lenses (L1 and L2) for demagnification on target. (b) Cross section of a 150-µm glass slide machined with a single pulse of ≈ 1 mJ energy. The SEM image reveals the formation of a channel.

References

[1] M. Duocastella and C. B. Arnold, "Bessel and annular beams for materials processing," *Laser Photon. Rev.*, vol. 6, no. 5, pp. 607–621, Sep. 2012.

[2] R. Gattass and E. Mazur, "Femtosecond laser micromachining in transparent materials," *Nat. Photonics*, 2008.

[3] I. Alexeev, K.-H. Leitz, a. Otto, and M. Schmidt, "Application of Bessel beams for ultrafast laser volume structuring of non transparent media," *Phys. Procedia*, vol. 5, pp. 533–540, Jan. 2010.

[4] D. Grojo, A. Mouskeftaras, P. Delaporte, and S. Lei, "Limitations to laser machining of silicon using femtosecond micro-Bessel beams in the infrared," *J. Appl. Phys.*, vol. 117, no. 16, p. In press, 2015.

[5] M. K. Bhuyan, F. Courvoisier, P. a. Lacourt, M. Jacquot, R. Salut, L. Furfaro, and J. M. Dudley, "High aspect ratio nanochannel machining using single shot femtosecond Bessel beams," *Appl. Phys. Lett.*, vol. 97, no. 8, p. 081102, 2010.

Determining the bilirubin concentration in bruises of human skin using spectral imaging

Marta Lange,[1] Inga Saknite,[1] Janis Spigulis[1]

[1]Biophotonics Laboratory, Institute of Atomic Physics and Spectroscopy, University of Latvia, Skunu Street 4 (Riga, LV-1003, Latvia)

***Corresponding author:** marta.lange.rtu@gmail.com*

The non-invasive diagnostics nowadays is one of the fields that is developing very fast. One of the most common uses of diagnostic tools is multi-spectral imaging using light at various wavelengths. This study shows comparison of multispectral and RGB imaging of bilirubin distribution changes over time in bruises. Other studies have shown tools to determine the age of a bruise by the use of spectral imaging and modelling. [1,2] The aim for this work is to analyse how is it possible to evaluate the bilirubin distribution in skin over time comparing the data acquired by multispectral imaging device *SkImager*, RBG imaging device and a smartphone.

The used methodology for this research is based on multispectral data cubes of a bruise that were acquired by multispectral imaging system Nuance CRi in the spectral range 450-950 nm with a spectral step of 10 nm. RGB data were acquired by an RGB imaging device *SkImager* that was developed at the Biophotonics Laboratory, Institute of Atomic Physics and Spectroscopy. *SkImager* acquires red, green and blue channel images at different illuminations: white, 460 nm, 530 nm, 665 nm, and 950 nm LEDs, respectively.

Afterwards the multispectral data analysis was done by using Beer-Lambert law to obtain relative concentration value distributions of skin chromophores: hemoglobin and bilirubin which is one of the end products of hemoglobin. The data was collected from the volunteers with 1st to 2nd skin type (By Fitzpatrick scale) who had controlled bruises on their skin where the chromophore bilirubin can be observed. The controlled bruises for the volunteers were caused by using mechanism of paintball gun and a standard sized ball. The experiment was done in a controlled way in order to cause the same trauma each time on various spots of the body, also the constant distance and force of the paintball was used. During the experiment none of the volunteers were hurt and no permanent damage of the skin was caused.

RGB imaging data analysis was done by comparing images of different channels and illuminations to obtain hemoglobin and bilirubin relative concentration distributions. Results of the used devices were compared and the conclusions and were made regarding the distribution of bilirubin distribution changes in human skin. This study is a great contribution in forensic medicine and non-invasive diagnostics field for future experiments in order to estimate the relative concentration of bilirubin to evaluate the approximate age of the bruise.

References

[1] Barbara Stam, Martin J C van Gemert, Ton G van Leeuwen,Maurice C G Aalders “3D finite compartment modeling of formation and healing of bruises may identify methods for age determination of bruises”. Medical & Biological Engineering 09/2010; 48(9):911-21. DOI:10.1007/s11517-010-0647-5

[2] L.L. Randeberg, I. Baarstad, T. Løke, A.M. Winnem, E.L.P. Larsen, P. Kaspersen, O.A. Haugen, L.O. Svaasand, “Hyperspectral imaging of bruised skin”, Proceedings of SPIE, Vol. 6078:100–110, 2006

Blood optical properties at various glucose level values in THz frequency range

S I Gusev*, M A Borovkova, E A Strepitov, and M K Khodzitsky

ITMO University, 49 Kronverksky Ave., St. Petersburg, 197101, Russia
Corresponding author: mail@gusev-spb.ru

Number of patients with diabetes is rapidly growing every day (230 million in 2010, 460 million is projected by 2025) [1]. The disease is characterized by a sharply increased risk of complications such as diseases of the cardiovascular system - up to 20 times [1]. The seriousness of complications straightly depends on the control of blood glucose levels. Now, the most common way of glucose measurement is made by glucometers that require making a finger puncture. It should be noticed that each puncture is skin roughening which means a risk of blood poisoning, as well as patient discomfort.

Using non-invasive techniques for measurement of glucose levels could reduce the amount of manipulations that can cause a risk for patients by 1500 per year. Various biomolecules have specific frequency signatures in the terahertz (THz) frequency range, which can reveal their presence and determine the concentration [2,3]. Therefore, the optical properties of blood were studied in the THz frequency range in order to develop the method of control the blood glucose level by time-domain THz spectroscopy. Dependences of refractive index on glucose concentrations and different times after blood sampling were obtained.

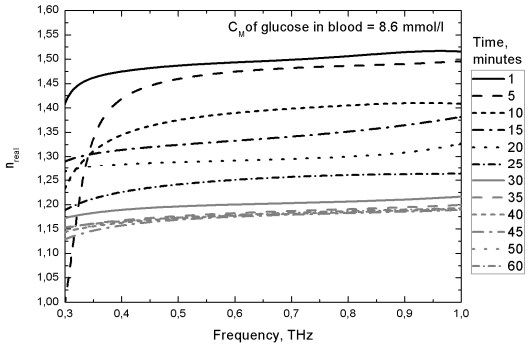

Fig. 1 Dependences of refractive index on different times after blood sampling.

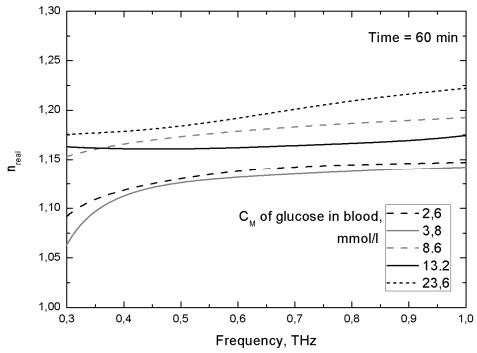

Fig. 2 Dependences of refractive index on glucose concentrations.

Double Debye model could be described by five Debye parameters: static dielectric constant (related to a zero frequency limit), optical dielectric constant (related to a high frequency limit), intermediate constant and two relaxation times for fast and slow processes [4,5]. Using this model the dispersion of complex dielectric permittivity of investigated object could be approximated with a high accuracy. The determination of these main parameters allows analyzing cellular processes in various biological objects. Moreover, by using the effective medium theory, the blood components concentrations of the samples were obtained [6]. The blood was considered as a compound of elements: cloth (in transmission geometry), water and the blood components. Hence, using permittivity of each of these components obtained from the experiment and with the help of the special iteration algorithm the concentrations of each of the components were estimated.

References

[1] Med74.ru, *Diabetes: facts and figures.* Link: http://www.med74.ru/articlesprint249.html
[2] Edward Philip John Parrott, Yiwen Sun, and Emma Pickwell-MacPherson, “Terahertz spectroscopy: Its future role in medical diagnoses”, Journal of Molecular Structure **1006.1** 66-76 (2011).
[3] Nazarov, M. M., et al, “Modification of terahertz pulsed spectrometer to study biological samples”, Saratov Fall Meeting 2006: Optical Technologies in Biophysics and Medicine VIII, International Society for Optics and Photonics (2007).
[4] Bao C. Q. Truong et al, “Debye Parameter Extraction for Characterizing Interaction of Terahertz Radiation With Human Skin Tissue”, IEEE Transactions On Biomedical Engineering, **60**, №6, pp. 1528-1537 (2013).
[5] Cecilie Rønne et al, “Investigation of the temperature dependence of dielectric relaxation in liquid water by THz reflection spectroscopy and molecular dynamics simulation”, Journal of Chemical Physics, **107, №14**, pp. 5319-5331 (1997).
[6] Gente R. et al. “Determination of leaf water content from terahertz time-domain spectroscopic data”, Journal of Infrared, Millimeter, and Terahertz Waves, **vol. 34. №. 3-4**, pp. 316-323 (2013).

Resonance Raman Spectroscopy in Twisted Bilayer Graphene

Eliel G.S.N[1]; RIBEIRO, Henrique[2], RIGHI, Ariete[1]; FANTINI, Cristiano[1]; SATO, Kentaro[3]; SAITO, Riichiro[4]; CHIU, Po-Wen[5]; PIMENTA, Marcos[1]

[1]Departamento de Física, Universidade Federal de Minas Gerais, 31270-901 , Belo Horizonte, MG, Brasil
[2]Mackgraph, Universidade Presbiteriana Mackenzie, 01302-907, São Paulo,
[3]Sendai National College of Technology, Sendai 989-3128, Japan
[4]Department of Physics, Tohoku University, Sendai, 980-8578, Japan
[5]National Tsing Hua University, Hsinchu 30013, Taiwan, Taiwan

***Corresponding author:** elielgsn@gmail.com*

The interest in 2D materials has increased in the last years, and nowadays the focus is making van der Walls devices by stacking 2D material layers. This comes with a challenge to understand this stacking effect, and how it modulates electronic and optical properties. One of those systems is two graphene layers with an angle mismatch known as twisted bilayer graphene (TBG). In our work we use resonance Raman spectroscopy to study the mismatch effect in TBG. Our goal is to show the resonance behaviour of two observed peaks in figure 1, the G band and the peak that appears around 1460 to 1520 cm^{-1}, associated to phonons of TO branch of graphene. We obtain for the first time the Raman resonance profile of G and TO branch for a group of samples. Using the G band information and tight binding calculations, we could correlate the resonance energy and the mismatch angle, the linear behaviour of the energy in respect to the angle agrees with the continuum model made by Dos Santos *et al.*[1]. Also the width of resonance provides us information about the width of the Van Hove singularities associated with this resonance process and the lifetime of the excited electronic levels. G and TO branch present a similar resonance energy, but the width of resonance is bigger to TO branch, it means that those phonons may have different intermediate states. Another point is try to use Raman as an angle measure technique, we correlate the information of the energy of Raman profile of the G band with the angle of the sample by finding the maximum of the resonance. On the other hand using a model presented by Carozo *et al.* [2]. We evaluate the angle dependence with the TO branch mode in figure 2. Since the TO branch has a wider resonance profile and accurate peak position, obtaining the relative rotational angle with TO branch peak is advantageous than G band.

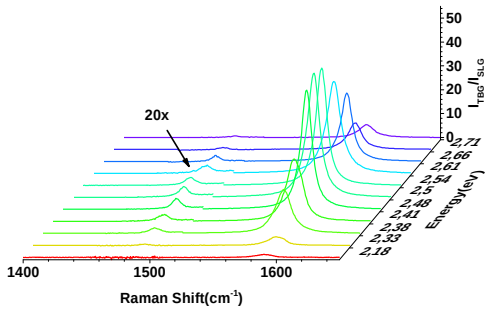

Fig. 1: Normalized Raman Spectra for a TBG graphene sample showing resonance profile.

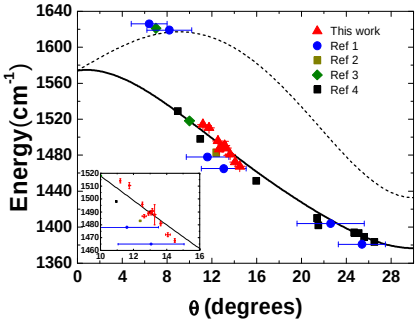

Fig. 2: LO and TO branchs energies in function of sample angle. Red points is our work, others come from references [2-5]

References

[1] J. M. B. Lopes dos Santos, N. M. R. Peres, and A. H.Castro Neto, "Graphene Bilayer with a Twist: Electronic Structure", Phys. Rev. Lett, 99, 256802 (2007)
[2] V. Carozo, C. Almeida, B. Fragneaud, P. Bedê, M. Moutinho, J. Ribeiro-Soares, N. Andrade, A. Souza Filho, M. Matos, B. Wang, et al., "Resonance effects on the Raman spectra of graphene superlattices", Physical Review B, **88**, 085401 (2013)
[3] R. W. Havener, H. Zhuang, L. Brown, R. G. Hennig, and J. Park, "Angle-Resolved Raman Imaging of Interlayer Rotations and Interactions in Twisted Bilayer Graphene"Nano letters **12**, 3162 (2012)
[4]K. Kim, S. Coh, L. Z. Tan, W. Regan, J. M. Yuk, E. Chatterjee, M. F. Crommie, M. L. Cohen, S. G. Louie, and A. Zettl, "Raman Spectroscopy Study of Rotated Double-Layer Graphene: Misorientation-Angle Dependence of Electronic Structure", Phys. Rev. Lett. **108**, 246103(2012).
[5] Y. Wang, Z. Su, W. Wu, S. Nie, N. Xie, H. Gong, Y. Guo, J. Hwan Lee, S. Xing, X. Lu, H. Wang, X. Lu, K. McCarty, S.-s. Pei, F. Robles-Hernandez, V. G. Hadjiev, and J. Bao, "Resonance Raman spectroscopy of G-line and folded phonons in twisted bilayer graphene with large rotation angles", Applied Physics Letters **103**, 123101 (2013).